The Institute for Solid State Physics
The University of Tokyo

Highlights of Joint Research

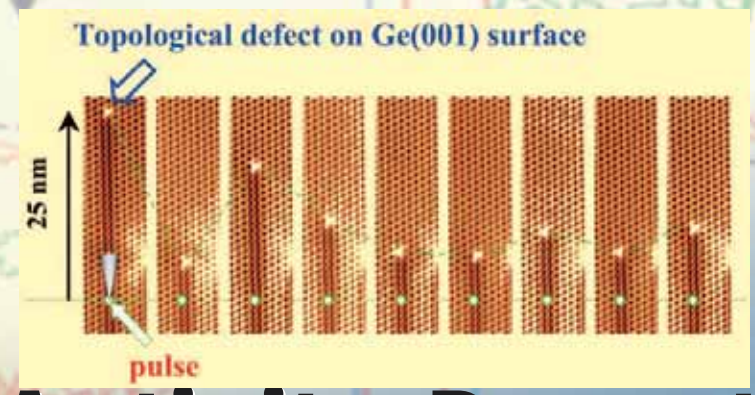

Activity Report 2005

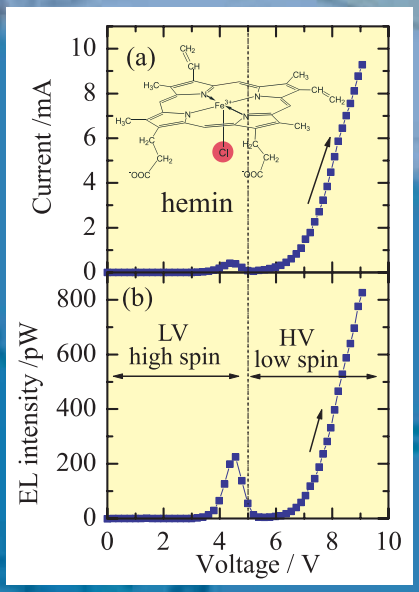

Highlights of Joint Research

Synchrotron Radiation Laboratory

The Synchrotron Radiation Laboratory (SRL) was established in 1975 as a research group dedicating to study solid state physics using synchrotron radiation. In 1989, the SRL started to hold the Tsukuba branch, a branch laboratory in the Photon Factory (PF), High Energy Accelerator Research Organization (KEK). SRL maintains an undulator called Revolver, two beamlines and three experimental stations; BL-18A for angle-resolved photoemission spectroscopy and two beamlines, BL-19A and BL-19B for spin-resolved photoelectron spectroscopy and soft X-ray emission spectroscopy experiments using undulator radiation. They are fully opened to outside users for experiments using high brilliant synchrotron radiation from the undulator. The operation time of these beamlines are about 5000 hours and the number of users is more than 200 a year.

The present SRL consists of the accelerator physics group and the solid state spectroscopy group. The members of the accelerator group have been carrying out research works on the accelerator physics and developing various new accelerator related technology in collaboration with other SR facilities. The spectroscopy group has been not only serving users at the Tsukuba branch with technical supports and advices, but also carrying out their own research works on advanced solid state spectroscopy.

In 2005, the operation of the PF ring was quitted from April to the end of September to improve its characteristics as a light source. Several straight sections were elongated, so that many insertion devises could be installed into the storage ring. The long term shut down of the PF ring reduced the scientific activities using synchrotron radiation at the Tsukuba branch. Instead, some of the staff members of SRL have made experiments at other SR facilities and some others have dedicated to improve experimental apparatuses at the beamlines, which results some new achievements. One is a new angle-resolved photoemission spectrometer with a high resolution analyser (PHOIBOS 150) and a equipment for sample preparation. The new system was commissioned already and will be installed at BL-19A in 2006. The other is a new inverse photoemission spectrometer for measuring unoccupied electronic states of solids and solid surfaces. They have observed an energy dispersion of unoccupied surface states of LaB_6(100) and showed that the low work function of the LaB_6(100) are originated from the charge redistribution at the surface.

Since 1980s, SRL has been promoting the "Super-SOR" project for constructing a new synchrotron radiation facility with a third generation light source dedicated to the sciences in vacuum ultraviolet and soft X-ray (VSX) regions. However, during last year, the president office of the university found out that the promotion of the project is very difficult or almost impossible for financial reasons. The budget for the new facility project is too big to be supported by a single university in Japan even after the reformation of the national universities. The decision of the president office was made the staff members of SRL to face to a great difficulty, and they started to find out a new direction of the solid state spectroscopy in VSX region.

After many discussions, SRL has inclined to construct beamlines using undulator radiation in other SR facilities instead of constructing the facility with a light source and to promote advanced materials sciences using high brilliance and small emittance of SR which have been considered in the Super-SOR project. They are those such as microscopy and time-resolved experiments which will only be possible using third generation light source and will promise us a considerable progress in the studies of nano-particles and real time observation of magnetic domains and of chemical reaction at catalytic surfaces, etc. The details of the future plan is not definite yet, however, we are planning to follow up the desire of the user community and to construct competitive beamlines for new scientific opportunities in VSX region using high brilliance SR.

The accelerator group studied feasibility of an energy-up of the Super-SOR light source for request of the university and found that the energy could be increased up to 2.4 GeV only with small modification and cost-up. They successfully designed the light source based on a 2.4 GeV storage ring and its injector (2.4 GeV booster synchrotron and 200 MeV linac), which satisfied the requirements of both material science and biotechnology, though the budget was still too big for the president office of the university to start the project in near future. They also developed the advanced accelerator component and subsystem such as the high-resolution beam profile monitor with zone plates, the one-cell magnet girder, the Java/CORBA control system, copper-plating insertion-device vacuum chamber, high-resolution beam position monitor and stabilization system and so on. Furthermore they started to collaborate with JAEA and KEK to develop a new accelerator system, an energy recovering linac (ERL), and to construct an ERL prototype in the KEK site in near future, which will be used as one of the best light sources in VSX region.

Neutron Science Laboratory

The Neutron Science Laboratory (NSL) has been playing a central role in neutron scattering activities in Japan since 1961 by performing its own research programs as well as providing a strong general user program for the university-owned various neutron scattering spectrometers installed at the JRR-3 operated by Japan Atomic Energy Agency in Tokai. In 2003, the Neutron Scattering Laboratory was reorganized as the Neutron Science Laboratory to further promote the neutron science with use of the instruments in JRR-3. Under the general user program supported by NSL, 14 university-group-owned spectrometers in the JRR-3

reactor (20MW) are available for a wide scope of researches on material science, and proposals close to 300 are submitted each year, and the number of visiting users under this program reaches over 6000 person-day/year.

Triple axis spectrometers and a high resolution powder diffractometer are utilized for a conventional solid state physics and a variety of research fields on hard-condensed matter, while in the field of soft-condensed matter science, researches are mostly carried out by using the small angle neutron scattering (SANS-U) and/or neutron spin echo (iNSE) instruments. The upgraded time-of-flight (TOF) inelastic scattering spectrometer is now opened to the user proposals.

Major research topics on the hard-condensed matter science cover stripe order in high-T_c superconductors, and closely related 2 dimensional systems, charge and orbital ordering in CMR manganites, quadrapolar ordering in rare-earth based intermetallic compounds, spin dynamics of low dimensional dimmer systems, etc. On the other hand, the research topics on the soft-condensed matter science cover structural characterization of polymer blends, micelles, amphiphilic polymers, block copolymers, liquid crystals, proteins, inorganic gels, dynamics of brush-polymers on surface, slow dynamics of surfactants, pressure dependence of dynamics of amphiphilic membranes, and so on. In addition, there are a variety of activities on fundamental physics, neutron beam optics, developments of neutron scattering techniques.

The NSL also operates the U.S.-Japan co-operative program on neutron scattering, providing further research opportunities to material scientists who utilize the neutron scattering technique for their research interests.

The details of individual studies and research hightlights in JFY2004 are reported in the NSL-ISSP Activity Report vol. 12.

Supercomputer Center

The supercomputer system in the Supercomputer Center of the Institute (SCC-ISSP) is placed at the service of general researchers of condensed matter physics through the User Program conducted by the Materials Design and Characterization Laboratory (MDCL). One of its aims is to selectively promote and support huge computations.

In March 2005, the SCC-ISSP renewed its main system which has two super-computers. Hitachi SR11000/48, called System-A, consists of 48 high performance nodes composed of tightly-coupled microprocessors. A node can be utilized as an uniprocessor computer by automatic parallelization of its Fortran compiler. System-A has 2.8 TB memory and achieves 5.8 TFlops peak performance in total. On the other hand, SGI Altix 3700/1280, called System-B, is a loosely-coupled parallel supercomputer consisting of 19 nodes inter-connected by a gigabit Ethernet network. Each node is a distributed-shared-memory-type computer consisting of 64 Intel Itanium 2 CPU's interconnected by a rather high performance network and have 64 GB memory. System-B achieves 7.7 TFlops total throughput performance.

A project can be proposed by any staff in universities or public research institutes in Japan. The projects proposed are judged by the Steering Committee of the SCC-ISSP, under which the Supercomputer Project Advisory Committee is formed to review proposals. In fiscal year 2005 totally 179 projects were approved. The total points applied and approved are listed on Table 1 below.

The research projects are roughly classified into the following three (the number of projects approved):

First-Principles Calculation of Materials Properties (72)
Strongly Correlated Quantum Systems (67)
Cooperative Phenomena in Complex, Macroscopic Systems (40)

All the three involve both methodology of computation and its applications. The results of the projects are reported in 'Activity Report 2005' of the SCC-ISSP. In the report the following four invited articles are included:

"Electronic Structure Calculations for Strongly Correlated Electron Systems", by T. Fujiwara *et al.*,
"A New Approach to First-Principles Calculation of Charged Surfaces", by M. Otani and O. Sugino,
"Numerical Study of Low Dimensional Quantum Spin Systems with Spatial Structures", by K. Hida,
"Particle-Dynamics Approach to Non-Equilibrium Phenomena", by F. Ogushi *et al.*.

Table 1: Research projects approved in 2005

Class	Max.Point	Application	# of Proj.	Total points			
				Applied		Approved	
				Sys-A	Sys-B	Sys-A	Sys-B
A	100k	any time	2	100K	100K	100K	100K
B	2M	twice a year	60	86.9M	27.55M	86.6M	27.55M
C	20M	twice a year	105	1210M	603.9M	962.8M	597.9M
D	none	any time	11	82M	179M	179M	147M
S	>20	twice a year	1	30M	5M	30M	5M

The maximum points allotted to the project of each class are the sum of the points for the two systems; 1 K point of System-A corresponds to charge for 0.37 hours × node, while the corresponding figure is 0.22 hours × 64CPU for System-B.

Synthesis of 3d Transition-Metal Nitrides under High Pressure in Supercritical Nitrogen Fluid

M. Hasegawa, K. Niwa, and T. Yagi

Synthesis of metal nitrides are much more difficult, compared to metal oxides, because they usually decompose at high temperatures. As a result, only limited studies have been so far made to clarify their physical properties, although they are expected to be quite interesting. Here we report synthesis of various metal nitrides using a new technique; a direct reaction between transition metal and supercritical nitrogen fluid under high pressure.

Diamond anvil cell (DAC) provides us powerful means to achieve very wide range of high pressures. By combining it with laser heating system (LASER-DAC), high temperature conditions above several 1000 K can also be achieved simultaneously, because the laser beam can permeate through the diamond anvil and is absorbed by the sample in the DAC. In other words, LASER-DAC can be a powerful tool to synthesize new materials under very wide P-T conditions and many geoscientists have applied this technique to study the Earth's deep interior. The DAC has another big advantage over large-volume high-pressure apparatus that gaseous materials can be compressed easily. By heating solidified gas under pressure, a supercritical fluid can be formed, which is highly reactive with various materials. Direct reactions using such supercritical fluid provides possibility to synthesize new materials which were difficult to make by other means.

We have reported crystal growth of GaN, which is one of the most famous nitrides because of its capability for a blue laser diode, in a supercritical nitrogen fluid at about 10 GPa using the LASER-DAC system [1]. High quality colorless transparent fine crystals of GaN in the wurtzite-type structure were grown from molten gallium and fluid nitrogen. Using the same experimental technique, we have also succeeded to synthesize Co_2N [2]. These results indicate that the LASER-DAC system opens us a new way of synthesis and crystal growth of variety of nitrides. The 3d-transition metal nitrides are attractive materials from the view point of materials science, because they exhibit variety of unique physical properties such as superconductivity, antiferromagnetism, ferromagnetism and so on, depending on the combination of elements. It is difficult to synthesize these nitrides, particularly for the late 3d-transition metals, by a simple direct nitriding reaction between nitrogen and metal at ambient pressure. The reported synthesis processes for these nitrides vary depending on the transition metal and it is not easy to study their properties systematically, such as their phase stability, crystal structures, and intrinsic defect of nitrogen.

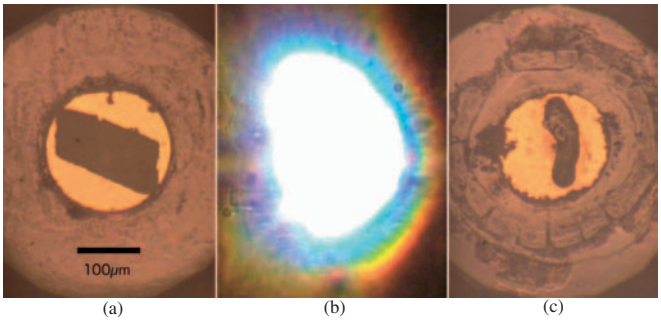

Fig. 1. Photographs of the sample in DAC before, during, and after (from left to right) the laser heating at 10 GPa. The sample was heated at about 1800 K.

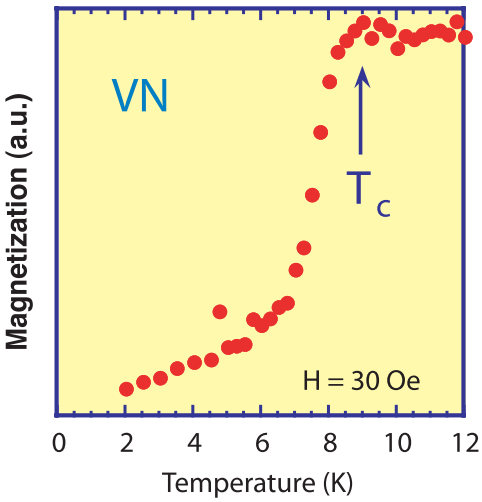

Fig. 2 Temperature dependence of magnetization of synthesized VN. The magnetization was measured by SQUID using one tiny sample. A superconducting transition is observed at about 9 K.

In the present study the syntheses of the 3d-transition metal nitrides have been tried by only one kind of reaction, *i.e.* a simple direct nitriding reaction between 3d-transition metal and supercritical nitrogen fluid at high pressures using the LASER-DAC system.

Small piece of transition metal (about 150 μm × 100 μm × 20 μm) was placed in the sample chamber of DAC together with the ruby pressure marker. The chamber was then filled with nitrogen gas of about 150 MPa and then closed. By increasing the applied load of the DAC, the sample chamber was squeezed and the pressure was increased to a desired value. Nitrogen in the sample chamber was solidified below 2 GPa. A multi mode YAG laser (100 W CW) was employed for heating and the laser beam was split into two by a half mirror to irradiate the sample from both sides of DAC to heat the sample homogeneously. The sample during heating was observed from both sides using two CCD cameras and recorded by the DVD recorder. Figure 1 is an example of the photographs of the sample before (a), during (b) and after (c) the laser heating at 10 GPa. The sample was heated at about 1800 K. The solid nitrogen was melted during the laser heating and this supercritical fluid has reacted with the transition metals directly. After the heating, the pressure was released and the reacted sample was recovered to ambient condition and was examined by X-ray diffraction. X-ray measurements were made at room temperature by a lab-based micro-diffractometer (Cr Kα) using a position sensitive proportional counter. All the 3d-transition metal nitrides, except Cu nitride, such as TiN, VN, CrN, Mn_3N_2, Fe_2N, Co_2N and Ni_3N were synthesized easily at the same condition described above [3]. This indicates that high-pressure and high-temperature synthesis in a supercritical nitrogen fluid using diamond anvil cell and YAG laser heating is highly useful to synthesize metal nitrides. The stoichiometry and the crystal structure changed systematically with the atomic number. The Ti, V and Cr form 1 to 1 compounds, TiN, VN and CrN, with NaCl-type structure. The Mn nitride is an IrU_2C_2-type nitrogen-rich non-stoichiometric Mn_3N_2. The Fe and Co nitrides are the PbO_2-type Fe_2N and CFe_2-type Co_2N, respectively, while the Ni nitride is the O_3Re-type Ni_3N. No Cu nitride was formed in the above condition. These results indicate that the ratio of nitrogen to metal, N/M, of the nitride decreases from 1 to 0 with the sequence from the early transition metal to the late transition metal. This means that in the 3d-transition

metals, nitriding reaction becomes more difficult with increasing the atomic number. The systematic change of the N/M ratio and crystal structure of the 3d-transition metal nitrides can be interpreted on the basis of the electron arrangement of the 3d-transition metal, which is relevant to its coordination number. Besides, the superconducting transition of the NaCl-type nitrides (TiN, VN) obtained by the present study were measured by the SQUID measurement of the magnetization [3]. Figure 2 is an example of such measurement and although the size of the sample synthesize by this technique is very small, it is clear that we can still measure these physical properties. It can be concluded from these results that the LASER-DAC is a powerful technique to synthesize novel metal-nitrides and study their property systematically. Taking this advantage, we are now making exploratory study of the synthesis of new nitrides using this technique.

References

[1] M. Hasegawa and T. Yagi, J. Crystal Growth **217**, 349 (2000).
[2] M. Hasegawa and T. Yagi, Solid State Commun. **135**, 294 (2005).
[3] M. Hasegawa and T. Yagi, J. Alloys and Compnd. **403**, 131 (2005).

Authors

M. Hasegawa[a] , K. Niwa, and T. Yagi
[a]Institute for Materials Research, Tohoku University

Compensation of the Effective Field in the Field-Induced Superconductor κ-(BETS)$_2$FeBr$_4$

S. Fujiyama and M. Takigawa

The organic charge-transfer-salts containing magnetic ions have been attracting strong interest since field-induced superconductivity (FISC) was discovered in λ-(BETS)$_2$FeCl$_4$ [1]. At zero magnetic field, this material shows simultaneous antiferromagnetic (AF) order of localized moments (spin 5/2) on Fe^{3+} ions and metal-insulator transition of π-conduction electrons on BETS molecules. A magnetic field destabilizes both the antiferromagnetic order and the insulating state. The FISC appears at high fields between 18 and 41 T [2]. This was suggested to be due to the Jaccrino-Peter (JP) mechanism [3]: if there is antiferromagnetic coupling between Fe spins and π-electrons, superconductivity is expected when the external field compensates the exchange field on π-electrons from Fe spins, minimizing the spin-Zeeman pair breaking effect.

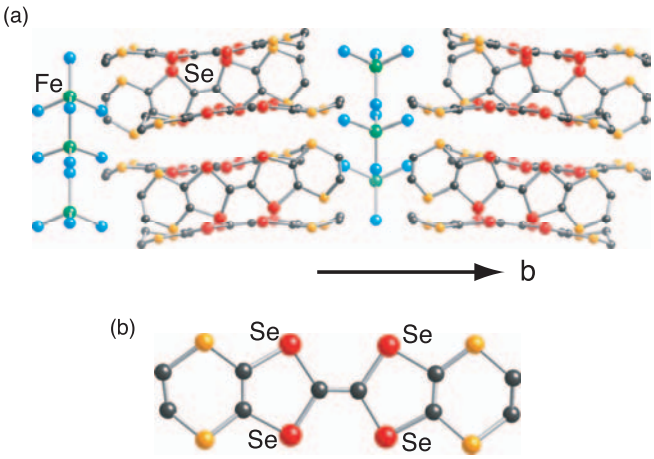

Fig. 1. (a) Crystal structure of κ-(BETS)$_2$FeBr$_4$ (b)Structure of BETS molecules.

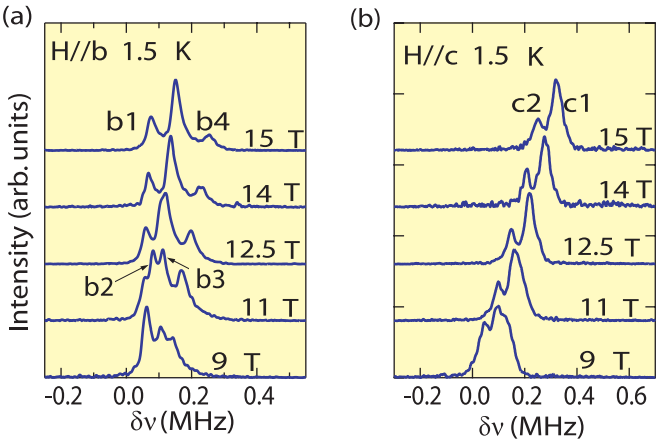

Fig. 2. ^{77}Se NMR spectra at T=1.5 K for the field along the b-axis (a) and the c-axis (b). The horizontal axes show the frequency shift from the resonance in diamagnetic materials.

The field-induced superconductivity has been observed also in the κ-type polymorph κ-(BETS)$_2$FeBr$_4$ for a much lower range of the field between 10 and 15 T [4] below 300 mK. Here we report the frequency shift of the ^{77}Se NMR in κ-(BETS)$_2$FeBr$_4$ to measure the spin polarization of the π-electrons. Our results demonstrate that the polarization of π-electrons at low temperatures vanishes for the field near 12 T, which is the central field for FISC, hence support the JP mechanism.

The crystal structure of κ-(BETS)$_2$FeBr$_4$ consists of alternating stacks of the conducting BETS layers and the insulating FeBr$_4$ magnetic layers (Fig. 1(a)). The four inequivalent Se sites in a molecule (Fig. 1(b)) are resolved in the NMR spectra for a single crystal at T=1.5 K (Fig. 2). The frequency shift δν has two contribution, $\delta\nu = \gamma_N A^{\pi}_{i,\alpha} m_\pi + \gamma_N (A^{dip}_{i,\alpha} + B_i) m_d$: the first term represents the contribution from the π-spin polarization m_π through the anisotropic hyperfine coupling $A^{\pi}_{i,\alpha}$ while the second term is due to the Fe magnetization m_d through the direct dipolar coupling $A^{dip}_{i,\alpha}$ and the transferred hyperfine coupling B_i. (γ_N is the nuclear gyromagnetic ratio.) Since $A^{dip}_{i,\alpha}$ can be calculated and m_d is completely saturated to 5 μ_B for the fields of our measurements, the dipolar field can be subtracted from the measured shift. The remaining shift $\delta\nu' = \delta\nu - \gamma_N A^{dip}_{i,\alpha} m_d = \gamma_N A^{\pi}_{i,\alpha} m_\pi + \gamma_N B_i m_d$ is plotted in Fig. 3 against the external field for various resonance lines.

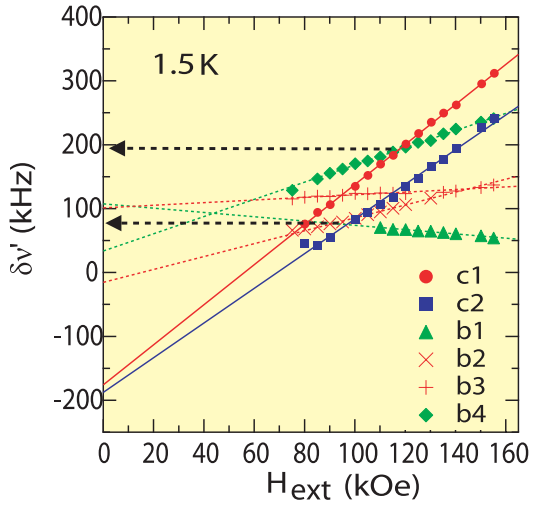

Fig. 3. Field dependence of the frequency shift of various resonance lines for H // b and H // c.

The linear relation between δν' and H_{ext} indicates validity of the mean field expression $m_\pi = \chi_\pi(H_{ext} + Jm_d)$ where Jm_d is the exchange field from Fe spins. If the compensation of the effective field occurs, m_π should vanish and δν' should become isotropic at the compensating field. Thus the value of the compensation field is known from the crossing of lines in Fig. 3 for H // b and H // c corresponding to the same sites. The plot in Fig. 3 indeed shows that such crossing occurs in the field range 10 – 12 T, supporting the JP mechanism. We also measured temperature dependence of the shift at a constant field. The analysis of the data lead to similar values of the exchange coupling between the Fe moments and the π-electrons. The consistent results from the two independent set of data provide convincing evidence for the JP mechanism of FISC in κ-$(BETS)_2FeBr_4$.

References

[1] S. Uji *et al.*, Nature **410**, 908 (2001).
[2] L. Balicas *et al.*, Phys. Rev. Lett. **87**, 067002 (2001).
[3] V. Jaccarino and M. Peter, Phys. Rev. Lett. **7**, 290 (1962).
[4] T. Konoike *et al.*, Phys. Rev. B **70**, 094515 (2004).
[5] S. Fujiyama *et al.*, Phys. Rev. Lett. **96**, 217001 (2006).

Authors

S. Fujiyama[a,b], M. Takigawa, J. Kikuchi[c], H-B. Chu[d,b], H. Fujiwara[d,b], and H. Kobayashi[d,b]
[a]Department of Applied Physics, University of Tokyo
[b]Crest-JST
[c]Department of Physics, Meiji University
[d]Institute for Molecular Science

Thermoelectric Power of a Quantum Dot in a Coherent Region

T. Nakanishi and T. Kato

A thermoelectric power (TEP) in mesoscopic systems has been of an important issue as another probe for electron transport properties. TEP in quantum-dot systems have been studied theoretically by the Landauer formula and master equations. Effects of electron-electron interaction have also been discussed by examining a deviation from the Mott formula. In these studies, however, coherency of the transmission through the quantum dot has not been fully considered. In recent experiments, the phase change by π between adjacent conductance peaks due to the zero transmission has been observed in an AB ring with a quantum dot [1]. It remains an important question to consider how TEP behaves around the zero transmission between conductance peaks.

In this study, we have considered the enhancement of TEP through the quantum dot in a coherent region [2]. It has been shown that a pronounced structure appears in a bias-voltage dependence of TEP due to the transmission zero. This indicates that TEP can be a good probe of the phase change between conductance peaks.

Within the Landauer formula, we have first derived the generalized Mott formula for TEP. The Sommerfeld expansion up to first order of the temperature T gives the (ordinal) Mott formula $S=-T\pi^2/(3e)\mathrm{d}(\log G)/\mathrm{d}\mu$, where G is a conductance. We here consider the system of the quantum dot with several quantum levels coupled to the leads. Assumed time reversal symmetry, the wave function in the quantum dot is chosen real. By neglecting the Coulomb interaction, one can obtain the transmission coefficient through the dot as a function of the bias voltage. By substituting this transmission coefficient to the Mott formula,

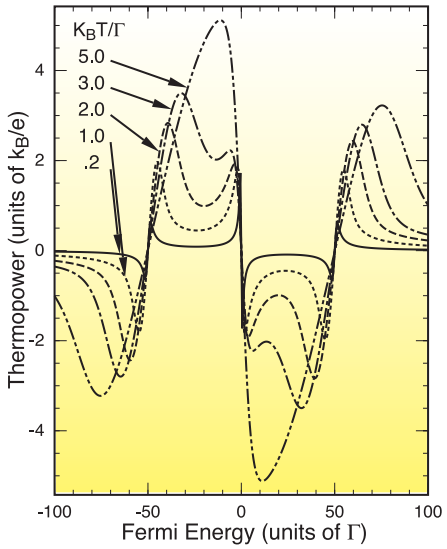

Fig. 1. Thermoelectric power (TEP) through the quantum dot with two levels at ε_1=-50Γ and ε_2=50Γ. As the temperature decreases, the bias-dependence of TEP changes from a sawtooth-like shape to one with characteristic peaks and dips at both the quantum levels (ε=ε_1, ε_2) and zero transmission point (ε=0) between the levels.

the bias-dependence of TEP is calculated as shown in Fig.1. Here, the quantum levels in the dot are located at ε_1=-50Γ and ε_2=50Γ, with Γ a level broadening. The significant enhancement of TEP can be seen around at the transmission zero point ε=0. The height of the peak and dip of the TEP around ε=0 approaches $\pi k_B/(3^{1/2}e)$~$1.81k_B/e$ at low temperatures. The prominent structure at ε=0 shows clearly the transmission zero, while it is hard to see it in the tail of the conductance.

Figure 2 shows TEP at low temperatures in the case of five conductance peaks at ε_n/Γ =100(n-3) for n=1~5, where the energy levels are indicated by arrows in the figure. The signs of the coupling amplitude between each quantum level and two leads include the phase information of the wave function inside the dot. Here, the coupling between left and right leads is taken as symmetric for n=1~4, while as

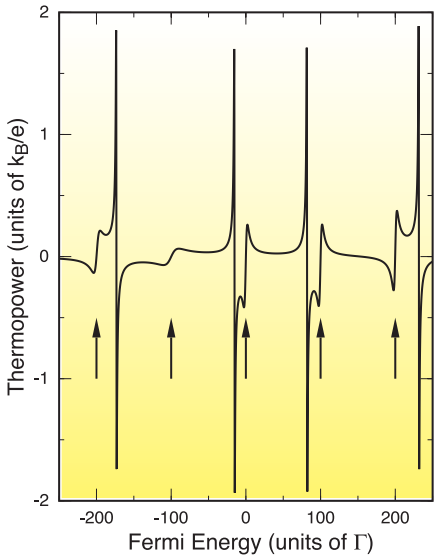

Fig. 2. Thermoelectric power (TEP) at the low temperature k_BT=0.2Γ. The arrows indicates the energy levels in the quantum dots. Between the quantum levels corresponding to the conductance peaks, characteristic structures with peaks and dips are observed. This structure may disappear as seen in the region between ε_4=100Γ and ε_5=200Γ. The presence of the peak and dip structure depends on the sign of the coupling between the dot and leads indicating the phase information of the wave function in the dot.

asymmetric for n=5. As shown in Fig. 2, TEP shows a sharp structure at transmission zero between the arrows for the in-phase case; three structures with peaks and dips are seen between the levels ε_n for n=1~4. The transmission zero, however, does not exist between ε_4 and ε_5, for the out-of-phase case. In the latter case, the transmission zero is outside of the peak; it corresponds to the sharp structure at ε~230Γ. Thus, the phase information can be indirectly obtained by measuring the bias-dependence of TEP at low temperatures.

In the present study, coherency between the dot and leads is essential. In real experiments, however, decoherence effects due to the environment may significantly affect the bias dependence of TEP. We expect that the present study will be naturally connected to the previous study based on incoherent processes like sequential tunneling and inelastic cotunneling [3] by introducing decoherence/dephasing mechanism.

References

[1] A. Yacoby, M. Heiblum, D. Mahalu, and H. Shtrikman, Phys. Rev. Lett. **74**, 4047 (1995).
[2] C. W. J. Beenakker and A. A. M. Staring, Phys. Rev. B **46**, 9667 (1992).
[3] M. Turek and K. A. Matveev, Phys. Rev. B **66** 115332 (2002).

Authors

T. Nakanishi[a] and T. Kato
[a]National Institute of Advanced Industrial Science and Technology

THz Emission from (Ga, Mn)As

J. B. Héroux, M. Kuwata-Gonokami, and S. Katsumoto

The quest for a THz light source with a high efficiency is an important issue in optics. It has been known that the THz radiation from non-magnetic semiconductors after excitation with a short light pulse is largely enhanced by applying an external magnetic field. The origin of the emission is the acceleration of excited carriers by built-in surface electric field or by diffusion. The external magnetic field bends the orbit of the carriers through Lorentz force, which improves the radiation coupling out of the sample. However, the application of a strong external field requires a large bulky system outside the source, which cannot be handled easily. In this work we observe that the "build-in" magnetic field in a ferromagnetic semiconductor (FMS) produces a similar effect on the THz radiation. The bending of charged carrier orbit with no external magnetic field in FMSs is often called anomalous Hall effect (AHE), the origin of which is now subject to renewed interest [1].

We have observed strong THz radiation from an FMS (Ga,Mn)As just after irradiation with light pulses [2]. The Mn content of the sample was 6% and the Currie temperature T_C was 110 K. The excitation pulse width was 130 fs with a central wavelength of 400 nm. Figure 1(a) shows typical results of a measurement of THz emission collected at normal incidence at 4.3 K, where the sample magnetization M is controlled by an external magnetic field B applied parallel to the sample surface. The polarization of the THz wave is linear and always perpendicular to the magnetization M in this configuration. A typical frequency-domain spectrum of the wave is shown in Fig. 1(b). Figure 1(c) shows curves of the peak THz intensity as a function of the B field strength

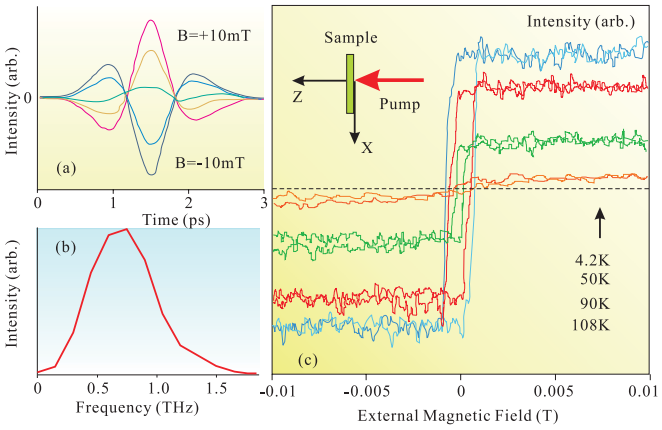

Fig. 1. (a) Typical experimental spectra of THz emission from GaMnAs in the time domain for a varying external B field. (b) Frequency domain spectrum. (c) THz hysteresis curves at varying temperatures. (4.2 K corresponds to the top curve in the right part of the graph.) Inset shows the axis definition and experimental configuration.

at varying temperatures. Clear temperature-dependent hysteresis curves are seen, and the signal could not be detected above T_C so that the emission is directly related to the existence of a ferromagnetic phase in the sample.

We have explained the results adopting a simple model based on a Drude-Lorentz equation of motion, in which the AHE is phenomenologically introduced. The observed strong enhancement of THz emission by ferromagnetism demonstrates the potential of diluted magnetic semiconductors for THz light source applications, and at the same time sheds light on the nature of AHE.

References

[1] T. Jungwirth, Q. Niu, and A. H. MacDonald, Phys. Rev. Lett. **88**, 207208 (2002).
[2] J. B. Héroux, Y. Ino, Y. Hashimoto, S. Katsumoto, and M. Kuwata-Gonokami, Appl. Phys. Lett. **88**, 221110 (2006).

Authors

J. B. Héroux[a], Y. Ino[a], Y. Hashimoto, S. Katsumoto, and M. Kuwata-Gonokami[a]
[a]Department of Applied Physics, University of Tokyo

Electronic States of Clean Ge(001) Surface

A. Ishii and F. Komori

The dangling bond states of the clean Ge(001) surface plays important roles in various dynamical phenomena at the surface, such as chemical reaction and electronic excitation. Recently, hot carrier dynamics is discussed on the basis of a topological defect motions induced by its local tunneling injection from the STM tip into the surface states [1]. However, the previous theoretical and experimental studies on the electronic structure were insufficient for the discussion on such hot carrier dynamics. Thus, we have investigated it using the band calculation based on the first-principles method, high-resolution ARPES and standing wave observations by STM.

The atomic structure of this surface is $c(4\times2)$ in the ground state as schematically shown in Fig. 1(a). The calculated surface band structure for this superstructure is shown in the upper panel of Fig. 2. The dangling bond empty π^* band is in the bulk band gap while the dangling bond filled π band is a resonance with the bulk states near Γ.

The valence band structure was measured by ARPES. We

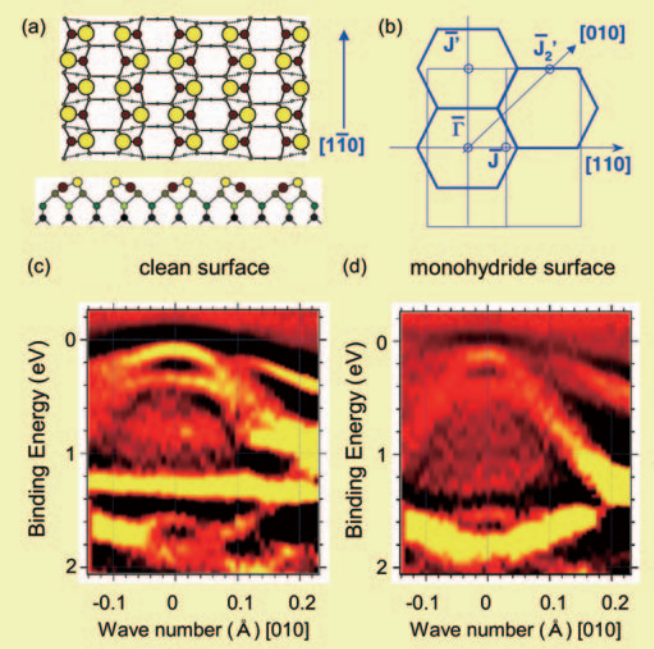

Fig. 1. (a) a schematic model of the $c(4\times2)$ surface structure. (b) The surface Brillouin zones for the $c(4\times2)$ (thick lines) and $p(2\times1)$ (thin lines) surfaces. (c,d) band dispersion around Γ observed at 130 K for the clean (c) and H-adsorbed (d) Ge(001) surfaces by ARPES.

found that the top band at Γ remains after adsorption of hydrogen atoms on the surface while the surface states clearly disappear as shown in Figs. 1(c, d). At temperatures higher than 470 K, the bottom of the π* band in the bulk band gap is thermally filled, and almost flat dispersion is detected by ARPES along the dimer-axis direction [Γ-J] as in the lower panel of Fig. 2. A large dispersion of the π* band in the direction perpendicular to the dimer-axis [Γ-J'] is obtained from the analysis of the standing waves observed at

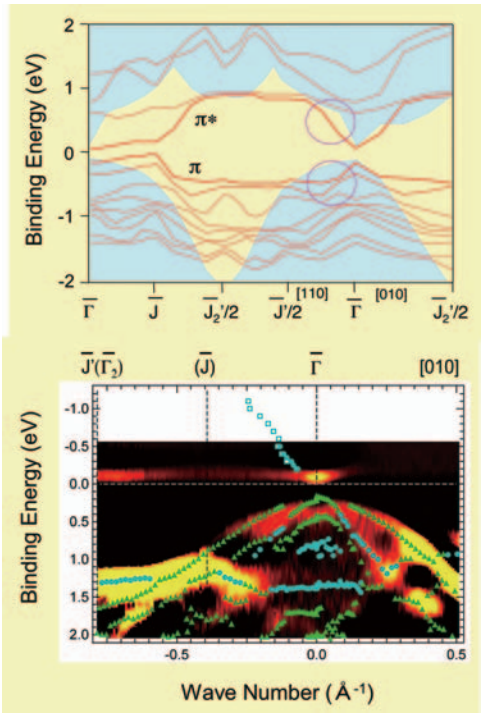

Fig. 2. Upper; Surface band structure for the clean Ge(001)-$c(4\times2)$ surface. The axes are defined for the 2×1 surface shown in Fig. 1(b). Blue areas indicate the bulk bands projected to the surface. Lower; band dispersion observed at 680 K for the clean Ge(001) surface by ARPES. Solid blue circles and green triangles indicate the surface and bulk states detected at 130 K. Open blue circles and squares above E_F are the states in the Γ-J' direction determined from the standing wave observation for the $c(4\times2)$ (circles) and $p(2\times2)$ (squares) surfaces.

80 K in differential conductance images of STM. All these experimental results agree well with the band calculation.

References
[1] Y. Takagi, Y. Yoshimoto, K. Nakatsuji, and F. Komori, J. Phys. Soc. Jpn. **74**, 3143 (2005).

Authors
K. Nakatsuji, Y. Takagi, H. Kusuhara[a], A. Ishii[a], and F. Komori
[a]Dep. Appl. Math. & Phys., Tottori University

Superconductivity of Nanometer-size Pb Islands Studied by Low-temperature Scanning Tunneling Microscopy

H. Sakata and Y. Hasegawa

When the size of superconducting materials becomes smaller than the coherence length of superconductivity, their superconducting properties are modified from the bulk. So far, various studies have been reported on superconductivity of nanometer-size particles. Detailed analysis has not, however, been successful since precise characterization of the size, shape and thickness of the particles has been difficult, and measuring the spatial variation of superconductivity within a single particle has been impossible. Using low temperature scanning tunneling microscopy (STM) we studied superconductivity of nanometer-size island structures by measuring tunneling spectra on the islands while characterizing the geometry of the islands from STM images [1]. Since all experiments including sample preparation were performed *in situ* under ultrahigh vacuum (UHV) conditions, unwanted effects of contamination or oxide layers can be eliminated.

As a sample, we chose Pb islands grown on Si(111) surface. Lead is one of the elemental superconductors with relatively high superconducting transition temperature (T_c = 7.2 K). We formed clean and well-characterized Pb islands on the semiconductor substrate and studied superconductivity *in situ* by taking tunneling spectra showing the superconducting gap to investigate how the superconductivity varies locally and how it depends on size and thickness of the Pb islands. For the measurements it is necessary to take the tunneling spectra far below T_c of the material. We used

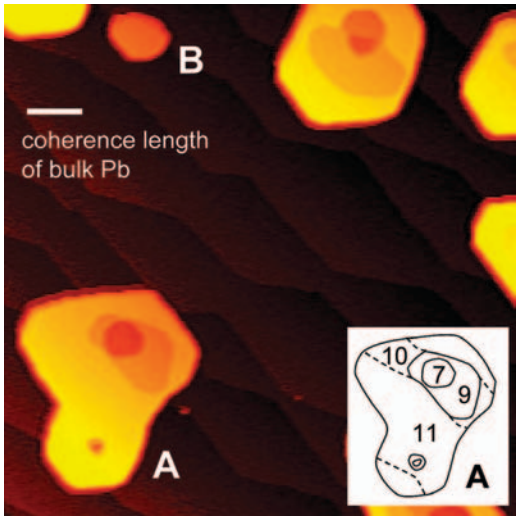

Fig. 1. STM image of Pb islands formed on Si(111) substrate. The size is 800 nm × 800 nm. The white line in the image corresponds to 87 nm, coherence length of bulk Pb. The inserts show local thickness of Pb on Island A. The thickness of Island B is 9 ML.

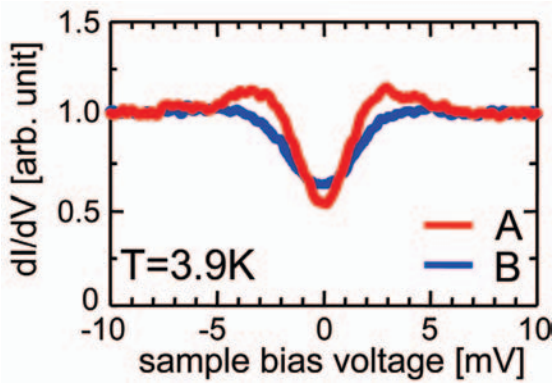

Fig. 2. Differential tunneling conductance spectra taken at 3.9 K on island A, whose diameter is larger than the coherence length, and island B, whose diameter is almost equal to the coherence length, are displayed.

low-temperature STM cooled by liquid ^{3}He, whose lowest temperature at the sample position is 1.2 K.

Figure 1 is an STM image of 4 ML Pb-deposited Si substrate showing several island structures on the surface. The islands are single crystal having a (111) plate on the top as the step height on the islands is multiple of the step height of Pb(111) (0.285 nm). From the height profile, the local thickness of the islands is measured, as is written with a small number in the inset drawings of Fig. 1. For convenience we named some Pb islands A, and B, as is marked in the STM image. The size of the islands is 58000 nm^2 for A, 5000 nm^2 for B. The coherence length of the bulk Pb superconductor is 87 nm.

First, we measured tunneling spectra showing the superconducting gap on various points in island A at 1.2 K. From the spectra it is found that all spectra taken on the island including the ones taken around the peripheral of the island have the same shape. A recent study reports thickness dependent superconductivity of Pb thin film on the same substrate. The same spectra independent of the thickness indicate that the superconductivity does not change within the nano-size Pb island, probably because the spatial variation of superconductivity is limited by the coherence length.

We then investigated its island dependence at various temperatures. Tunneling spectra measured on the two islands, A and B at 3.9 K are shown in Fig. 2. It is found from the figure that the shape of the tunneling spectra depends on the measured islands and that the dependence is enhanced at the higher temperature. The gap measured on the nano-size islands is larger than the bulk Pb value (1.35 meV). The smaller island shows the larger gap and the gap of the small island (B) increases with the temperature.

These peculiar properties are due to the superconducting fluctuation, we speculate. For the superconducting materials whose dimension is small the thermal fluctuation is significant and the effect is enhanced as the size becomes smaller and the measured temperature is higher. According to the theory which handles superconductivity of small particles, the gap is enhanced for smaller islands and at higher temperature because of the fluctuation, which is consistent with our results.

References

[1] T. Nishio, M. Ono, T. Eguchi, H. Sakata, and Y. Hasegawa, Appl. Phys. Lett. **88**, 113115 (2006).

Authors
T. Nishio, M. Ono, T. Eguchi, H. Sakata[a], and Y. Hasegawa
[a]Tokyo University of Science

Spin Flow Dynamics in Magnetically-Polarized Superfluid ^{3}He

H. Kojima and H. Ishimoto

When liquid ^{3}He is cooled in a magnetic field to low enough temperatures, the normal liquid first makes a transition into superfluid A_1 phase at T_{c1} and then into superfluid A_2 phase at a lower temperature T_{c2}. The most important aspect of the A_1 phase is that its superfluid component is totally spin-polarized along the magnetic field. It is a kind of ferromagnetic superfluid. A mass superflow is then simultaneously a spin flow. The phase transition into the A_1 phase is accompanied by the spontaneous breaking of relative spin-gauge symmetry. Interesting hydrodynamic effects occur in the A_1 phase such as a unique magnetic fountain pressure effect which was predicted by Liu [1] and established by Kojima [2]. Nevertheless earlier experiments on this interesting magnetically driven superflow have uncovered puzzling problems [3]. To clarify these, the magnetic fountain detector should be placed in the sample cell containing only A_1 phase liquid without interfaces with any other superfluid and normal phase. To realize such conditions, the ISSP nuclear refrigerator has been employed owing to its large experimental space and high magnetic field capability up to 15 T (originally in the frame of JSPS-NSF joint scientific program). A newly designed magnetic fountain pressure cell was constructed in which a large reservoir is connected to a small detector chamber through a super leak made of several channels 10 μm wide (Fig. 1). When magnetic field gradient is applied across the superleak, a magnetic fountain pressure is induced by spin-polarized superfluid flow. From the observed decay of the fountain pressure, spin relaxation time was determined between 1 and 29 bar and 0.2 and 8 T. The observed relaxation time τ is shown in Fig.2 as a function of reduced temperature $(T_{c1} - T)/(T_{c1} - T_{c2})$. It varies from less than 1 sec near T_{c2} to about 80 sec near T_{c1}. Surprisingly τ tends to vanish towards T_{c2} at all magnetic fields. To our knowledge, there is no theory which predicts such increase in relaxation rate over a relatively large temperature range near T_{c2}. A preliminary interpretation is given in terms of intrinsic spin relaxation based on Leggett and Takagi theory [4] and the predicted small but increasing presence of minority spin pair condensate in A_1 phase.

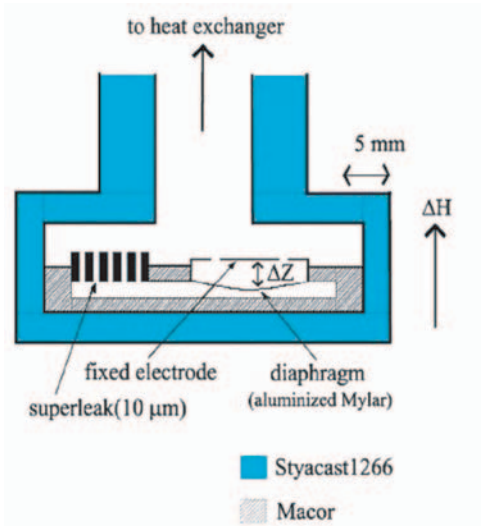

Fig. 1. Magnetic fountain pressure cell

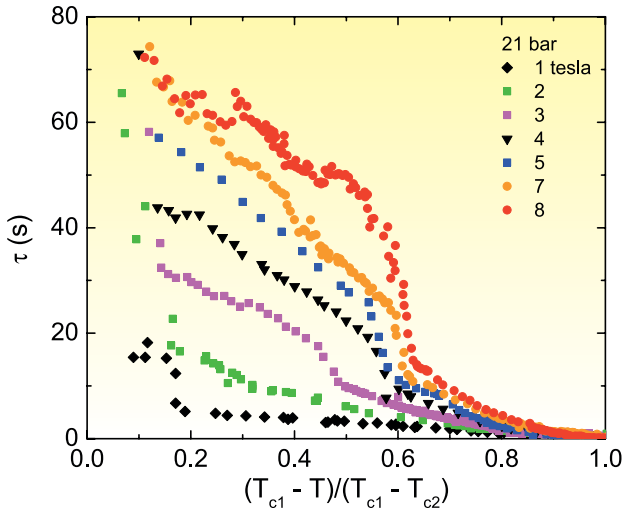

Fig. 2. Nominal spin relaxation time as a function of reduced temperature at various magnetic fields.

References
[1] M. Liu, Phys. Rev. Lett. **43**,1740 (1979).
[2] R. Ruel and H. Kojima, Phys. Rev. B **28**,6582 (1983).
[3] S. T. Lu, Q. Jiang, and H. Kojima, Phys. Rev. Lett. **62**, 1639 (1989).
[4] A. J. Leggett and S. Takagi, Annals of Physics **106**, 79 (1977).

Authors
A. Yamaguchi, S. Kobayashi, H. Ishimoto, and H. Kojima[a]
[a]Serin Physics laboratory, Rutgers University

Multistep Magnetization of Triangular Lattice Antiferromagnet $CuFe_{1-x}Al_xO_2$ in High Magnetic Fields

H. Aruga Katori, S. Mitsuda, and K. Kindo

Delafossite-type compound $CuFeO_2$ with layered structure of triangular lattices has been extensively investigated as one of the model materials of a triangular lattice antiferromagnet with geometrical spin frustration. Although the orbital singlet Fe^{3+} (L=0, S=5/2) magnetic ions have Heisenberg spin characters, $CuFeO_2$ shows exotic magnetic orderings with quasi-Ising character.

Recently, the effect of nonmagnetic Al^{3+} impurities on the magnetic orderings of $CuFeO_2$ has been investigated using single crystals $CuFe_{1-x}Al_xO_2$. The Al^{3+} concentration x versus temperature phase diagram is shown in the inset of Fig. 1 [1]. The Al^{3+} impurities cause the dramatic change of the ground state of $CuFeO_2$ by disturbing the delicate balance of the competing exchange interactions. The commensurate four-sublattice (4-sub) phase with quasi-Ising character is vanished by the substitution of the critical concentration x_c~0.014. The low-temperature (LT) phase of the samples with $0.015 \le x < 0.035$ is a complex incommensurate spin state. The samples with $x \ge 0.035$ undergo the oblique partial disordered (OPD) phase at low temperatures. In order to clarify the magnetic properties of the samples in the 4-sub, LT and OPD phases, we measured the magnetization of single crystals of high quality $CuFe_{1-x}Al_xO_2$ in high magnetic fields.

Figure 1 shows the magnetization curves $M(H)$ of the samples with various x. The sample with no impurity (x=0.000) shows multistep phase transitions. We found various changes of spin structures of $CuFeO_2$, from collinear to noncollinear, from noncollinear to collinear, and from collinear to collinear structure, depending on the strength of H. By the previous studies the spin structures have been determined in each field-induced phase as follows. In the first field-induced phase, spins establish a complicated incommensurate structure, which is called a five-sublattice-like (5-sub-like) phase tentatively. In the second, spins on the c-plane establish the commensurate five-sublattice (5-sub) structure parallel to the c-axis. In the third, the commensurate three-sublattice (3-sub) structure is established. Above 32 T we found a linear increment of $M(H)$, indicating a noncollinear spin structure. We call this region a fourth field-induced (4th) phase.

Multistep magnetization processes similar to $CuFeO_2$ were observed for the samples with $x \le 0.025$. However magnetic plateaus originating from a collinear spin structure becomes less pronounced when x is increased. For the samples with x=0.035 and 0.050 where the OPD phase is established in H=0, no field-induced phases was observed. Here we focus on the effect of Al^{3+} impurities in each field-induced phase.

The 4-sub phase. This phase appears in the samples with x<0.015, which is consistent with the fact x_c~0.014. In the samples with x=0.010 and 0.012, however, when H is decreased from high fields, $M(H)$ decreases with the same slope as in the 5-sub-like phase. It implies that the 5-sub-like spin structure is kept down to H=0 once it is established by applying high magnetic fields.

The 5-sub-like phase. The slope of $M(H)$ in this phase does not depend on x up to 0.025. Moreover, it has been confirmed that the LT phase of the sample with x=0.020 continues up to around 10 T by the neutron diffraction experiments [2]. Then we deduce that the 5-sub-like phase will be identified with the LT phase.

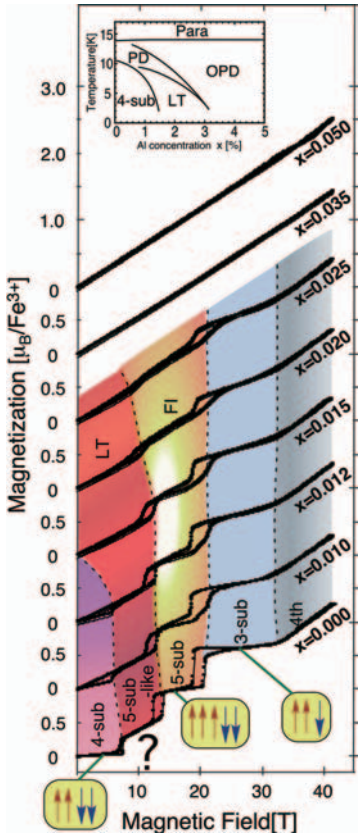

Fig. 1. Magnetization curves of single-crystal $CuFe_{1-x}Al_xO_2$ with various x measured at 1.6 K. The magnetic field was applied parallel to the c-axis. The inset shows the Al^{3+} concentration versus temperature phase diagram.

The 5-sub phase. This phase is strongly affected by impurities. The collinear spin structure seems to be destroyed by a small amount of Al^{3+} impurity. By increasing x, the noncollinear spin structure becomes to be constructed, which was observed in the region called a field-induced (FI) phase in the sample with x=0.020 [2].

The 3-sub phase. This phase is observed for the samples with $x \leq 0.025$. The collinear 3-sub spin structure is stronger against the Al^{3+} impurities than other collinear 4-sub and 5-sub spin structures.

The 4th phase. The slope of $M(H)$ does not change up to x=0.025, indicating that this noncollinear spin structure is stable.

References

[1] N. Terada, S. Mitsuda, T. Fujii, K. Soejima, I. Doi, H. Aruga Katori, and Y. Noda, J. Phys. Soc. Jpn. **74**, 2604 (2005).

[2] N. Terada, S. Mitsuda, K. Prokes, O. Suzuki, H. Kitazawa, and H. Aruga Katori, Phys. Rev. B **70**, 174412 (2004).

Authors

H. Aruga Katori[a], H. Mitamura, S. Kanetsuki[b], N. Terada[b], S. Mitsuda[b], K. Kindo, and S. Takeyama

[a]RIKEN

[b]Department of Physics, Tokyo University of Science

Pressure-Induced Spin Density Wave from Local-Moment Antiferromagnetism in Heavy Fermion $Ce_{1-y}La_y(Ru_{0.85}Rh_{0.15})_2Si_2$

S. Murayama, T. Nakano, and Y. Uwatoko

Typical heavy-fermion compound $CeRu_2Si_2$ shows different types of antiferromagnetic ordering by substitution of each Ce-, Ru- and Si-site by its particular second element. $Ce(Ru_{1-x}Rh_x)_2Si_2$ shows an incommensurate spin density wave (SDW) transition with partial gap on the Fermi surface along the c-axis due to the Fermi surface nesting in the heavy-fermion band [1, 2]. The gap opening is clearly observed from a gap-like jump in resistivity only along the c-axis [2]. $Ce_{1-y}La_yRu_2Si_2$ shows an antiferromagnetic (AF) ordering with different wave vectors and rather large magnetic moment [3]. Recently, we have measured the susceptibility and resistivity of $Ce_{1-y}La_y(Ru_{0.85}Rh_{0.15})_2Si_2$ in various La concentrations y [4, 5]. We found that the Kondo temperature T_K decreases rapidly and that the gap-like jump in resistivity disappears with increasing y as shown in Fig. 1(a). These results suggest that the La substitution introduces decrease of the c-f hybridization due to the negative chemical pressure and that the SDW changes to a local-moment-type AF (LAF) phase without any gap opening. In order to make clear the magnetic phase of this $Ce_{1-y}La_y(Ru_{0.85}Rh_{0.15})_2Si_2$ system, we have done detailed resistivity measurements under hydrostatic pressure.

Fig. 1(b) shows the temperature dependence of the resistivity of $Ce_{1-y}La_y(Ru_{0.85}Rh_{0.15})_2Si_2$, y = 0.25 along the c-axis under hydrostatic pressure. We observe a downward bend in resistivity at around the Néel temperature T_N for P = 0, which is usually observed at the normal AF transition. With increasing pressure, the bending at T_N becomes small and the gap-like jump occurs at P ≥ 0.43 GPa. With further increasing P, the jump disappears at P ≥ 1.16 GPa with a large T^2 term observed in the low temperature limit. We conclude from these results that an SDW with partial gap on

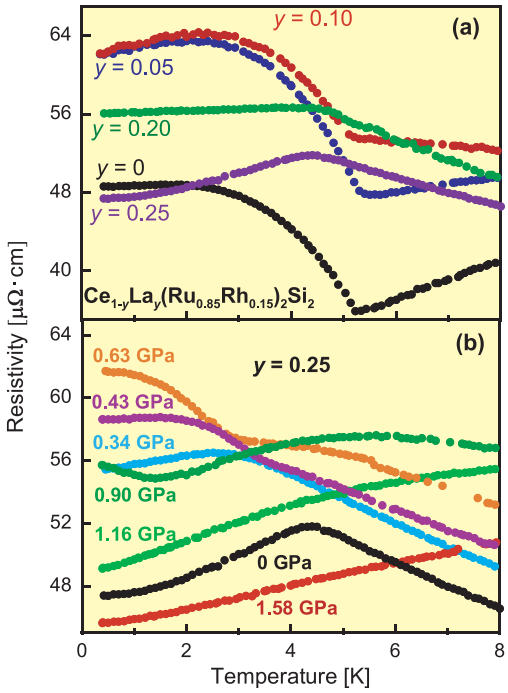

Fig. 1. Temperature dependence of the resistivity of $Ce_{1-y}La_y(Ru_{0.85}Rh_{0.15})_2Si_2$ along the c-axis. (a) shows the variation on the La concentration y and (b) shows the variation under hydrostatic pressure for y = 0.25.

the Fermi surface of the heavy fermion band is induced by pressure from the LAF phase of $Ce_{1-y}La_y(Ru_{0.85}Rh_{0.15})_2Si_2$, y = 0.25. This is just the opposite direction to the case of chemical La substitution. For P ≥ 1.16 GPa, the SDW gap disappears and typical Fermi-liquid (FL) state remains with a large effective mass. The present system can be one of the good candidates for the Doniach picture concerning the competing Kondo effect and RKKY interaction.

Figure 2 shows the magnetic phase diagram as a function of the La concentration y, pressure, and temperature determined from the susceptibility and resistivity. It is shown that the La substitution is always destructive for the SDW or FL phases. On the other hand, hydrostatic pressure plays a constructive role for the SDW or FL. This conflicting tendency can be well explained by change of the c-f hybridization due to the negative pressure by the La substitution and the positive hydrostatic pressure.

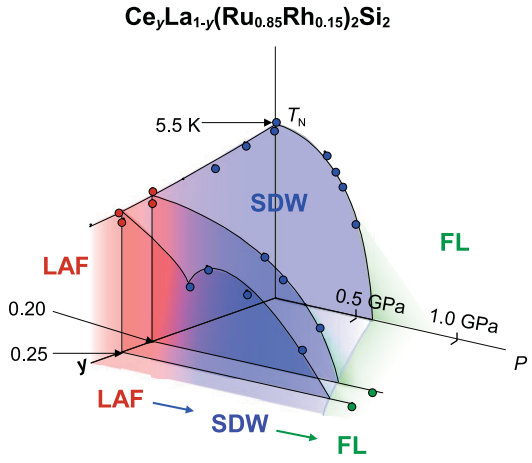

Fig. 2. Three-dimensional magnetic phase diagram of $Ce_{1-y}La_y(Ru_{0.85}Rh_{0.15})_2Si_2$ as a function of the La concentration y, pressure P, and temperature T determined from the susceptibility and resistivity.

Unfortunately, the mechanism of the Fermi surface nesting in the heavy-fermion band for the present system is still not clear, because there is no direct observation of the Fermi surface or band calculation except for $LaRu_2Si_2$ and $CeRu_2Si_2$. The nesting condition may be very delicate depending on the electron number and band state for 4f- and 4d-electrons. We need exact band investigation for $Ce_{1-y}La_y(Ru_{0.85}Rh_{0.15})_2Si_2$ to study further. Another interesting point to solve is the cross-over between the LAF and SDW. Is it a quantum phase transition or coexistence of the two phases? The present resistivity of $Ce_{1-y}La_y(Ru_{0.85}Rh_{0.15})_2Si_2$, y = 0.25 shows clear change between the downward bend and gap-like jump in resistivity by both the La substitution and hydrostatic pressure, and no definite evidence of the coexistence. This system may be also one of the good examples for the quantum phase transition under pressure.

References

[1] S. Kawarazaki, M. Sato, H. Kadowaki, Y. Yamamoto, and Y. Miyako, J. Phys. Soc. Jpn. **66**, 2473 (1997).
[2] S. Murayama, C. Sekine, A. Yokoyanagi, K. Hoshi, and Y. Onuki, Phys. Rev. B **56**, 11092 (1997).
[3] S. Quezel, P. Burlet, J. L. Jacoud, L. P. Regnault, J. Rossat-Mignod, C. Vettier, P. Lejay, and J. Flouquet, J. Magn. Magn. Mater. **76-77**, 403 (1988).
[4] T. Nakano, H. Yamashiro, K. Fujita, and S. Murayama, J. Phys. Soc. Jpn. **74**, 1602 (2005).
[5] A. Isoda, S. Shimada, Y. Kanda, S. Murayama, H. Takano, T. Nakano, M. Hedo, and Y. Uwatoko, Physica B, **359-361**, 169 (2005).

Authors

S. Murayama[a], T. Nakano[b,c], S. Shimada[a], T. Horii[a], M. Hedo, and Y. Uwatoko
[a]Muroran Institute of Technology
[b]Waseda University
[c]Japan Science and Technology Agency/CREST

Two-Peak Structure of Superconductivity in a Doped-Type Organic Superconductor

H. Taniguchi and Y. Uwatoko

The most well-known ambient-pressure organic superconductors, κ-(BEDT-TTF)$_2$X (X=Cu(NCS)$_2$ and Cu[N(CN)$_2$]Br etc.), can be regarded as a bandwidth-controlled superconductor at fixed band filling [1]. This is because, in these systems, the superconductivity is realized by pressurizing the Mott insulator. In this case, with increasing pressure, the electrons localized at dimers of BEDT-TTF experience the first-order insulator-metal or insulator-superconductor transition [2] and show Fermi liquid behavior [3] just as they start to delocalize.

The (BEDT-TTF)$_4$Hg$_{2.89}$Br$_8$ are also known to crystallize into the κ-type structure [4]. However, there is a peculiar structural characteristic not seen in other κ-type salts. This salt has incommensurate structure between lattice periodicity of mercury chains and that of donor molecules [4]. Due to this incommensurability of mercury ions, the electron filling is possibly shifted from the usual half-filled state of 2:1 salts. Therefore, kind of hole-doped state may be realized. Indeed this salt shows metallic temperature variation and superconductivity at 4.3K [4] even at ambient pressure in spite of highly enhanced U/W value (U/W=1.79). So we believe that the metallic and superconducting states of this Hg$_{2.89}$Br$_8$ salt are caused by the effect of "natural doping". In this sense, the Hg$_{2.89}$Br$_8$ salt offers the possibility of making a connection between other κ-type organics and the cuprates. In order to clarify the difference in physical properties between doped and nondoped organic superconductors, we measured resistivity of κ-(BEDT-TTF)$_4$Hg$_{2.89}$Br$_8$ as functions of temperature and pressure.

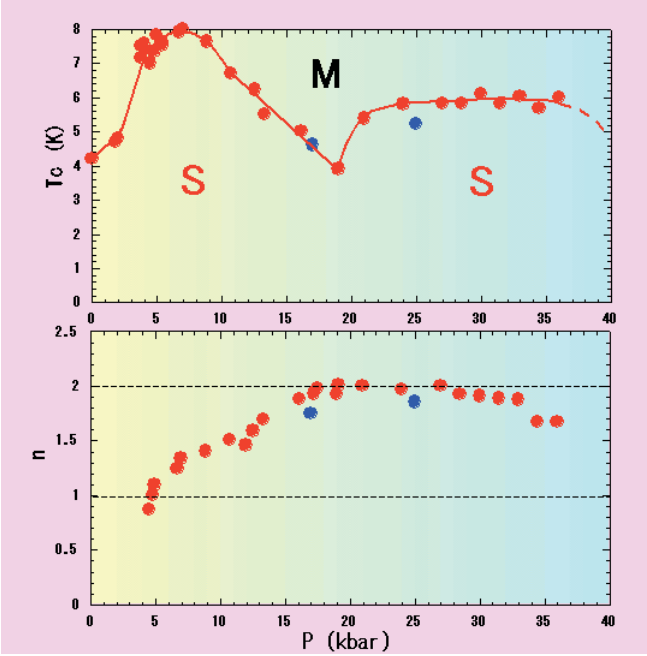

Fig. 1. Temperature-pressure phase diagram (upper panel) and pressure dependence of the power in the normal state resistivity (lower panel) of κ-(BEDT-TTF)$_4$Hg$_{2.89}$Br$_8$. The resistivity data were obtained by using a piston-cylinder-type pressure cell (red symbols) and the cubic anvil press in Uwatoko laboratory (blue symbols).

The electrical resistivity measurements were performed by using a piston-cylinder-type pressure cell and the cubic anvil press (Uwatoko laboratory). The obtained phase diagrams are displayed in Fig. 1. One of the most remarkable feature is pressure-insensitive nature of T_c. Pressure derivative of T_c at the intermediate-range, for example, is −0.45 K/kbar, of which absolute value is far smaller than approximately |-2| K/kbar of other κ-type materials'. This feature may suggest that the present superconductor is not a bandwidth-controlled type superconductor but a doped-type one.

More importantly, there is a two-peak structure in the T_c diagram. Such behavior has never been observed in other organic system and quite unusual. We found that the low temperature part of the resistivity data in the metallic state were well fitted by $R=R_0+T^n$ just before superconducting transition. The obtained n is shown in the lower panel. As observed in the figure, value of the power at the lowest pressure is approximately unity. This power is not seen in other organic systems and is reminiscent of anomalous metallic state of underdoped cuprate or rare earth conpounds near quantum critical point. With increasing pressure, the power gradually increases toward almost two and becomes almost stable around two over the higher-pressure superconducting phase. This behavior may reflect that the system undergoes a crossover or a transition to the Fermi liquid state. By applying pressure of 42.5 kbar, the superconductivity disappears within the measured temperature-range.

In summary, we observed quite unusual T_c-behavior in the doped-type organic superconductor. In addition, we found that transport properties showed strong violation from ones of other nondoped organic superconductors. We believe that the present organic salt is laid on the unique situation with the unique values of U/W and doping rate. Therefore,

the observation of two-peak structure of T_c and a crossover or a transition between the two superconducting phases are an important finding for the profound physics of the highly correlated electron system.

References

[1] K. Kanoda, Hyperfine Interact. **104**, 235 (1997).
[2] S. Lefebvre, P. Wzietek, S. brown, C. Bourbonnais, D. Jerome, C. Meziere, M. Fourmigue, and P. Batail, Phys. Rev. Lett. **85**, 5420 (2000)
[3] T. Ishiguro, K. Yamaji, and G. Saito, *Organic Superconductors* (Springer-Verlag, Berlin) 2nd Ed.
[4] R. N. Lyubovskaya, E. I. Zhilyabva, S. I. Pesotskii, R. B. Lyubovskii, L. O. Atovmyan, O. A. D'yachenko, and T. G. Takhirov Pis'ma Zh. Eksp. Teor. Fiz. **46**, No. 4, 149 (1987).

Authors

H. Tanigcuhi[a], N. Nagai[a], T. Okuhata[a], K. Satoh[a], M. Hedo, and, Y. Uwatoko

[a]Saitama University

Change of the Electronic States under Pressure in Ferromagnet CePtAl

M. Nakashima and Y. Uwatoko

Cerium and uranium compounds form heavy fermions at low temperatures, which is a consequence of competition between the Ruderman-Kittel-Kasuya-Yosida (RKKY) interaction and the Kondo effect. High pressure is useful in tuning the electronic states in these compounds. When pressure is applied to the magnetically ordered cerium and uranium compounds, the ordering temperature T_{mag} decreases and becomes zero at a critical pressure $P = P_c$. CePtAl crystallizes in the orthorhombic TiNiSi-type structure. There

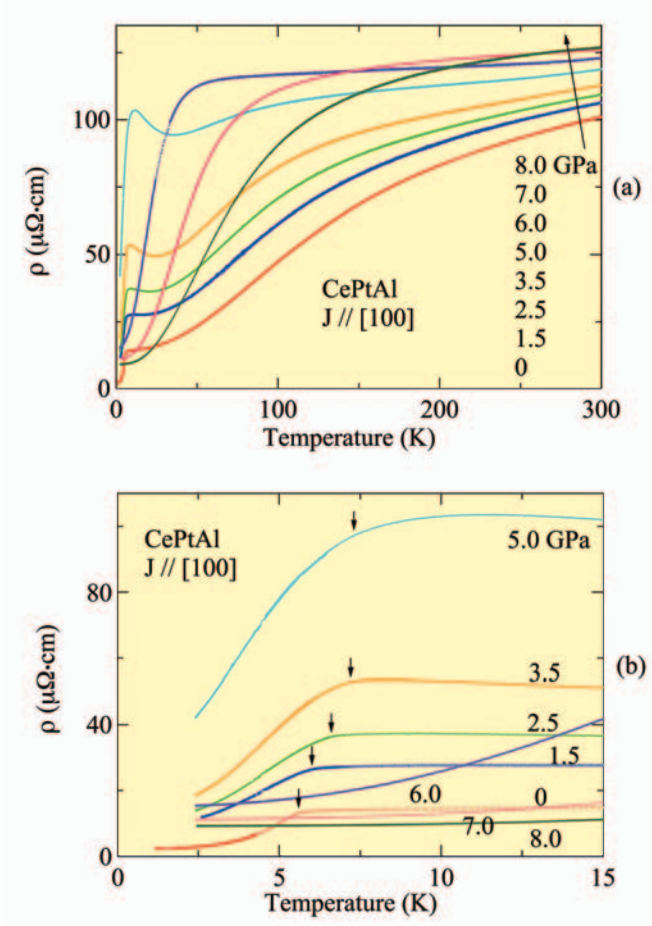

Fig. 1. Temperature dependence of electrical resistivity at several pressures in CePtAl. Arrows indicate the magnetic ordering temperature.

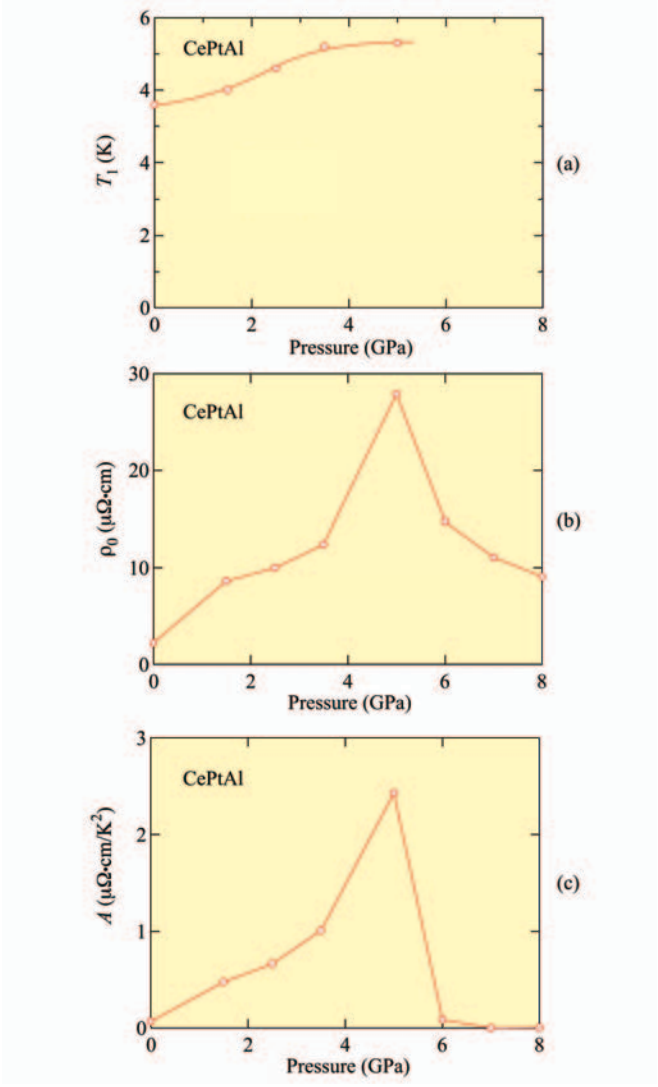

Fig. 2. Pressure dependences of T_1, ρ_0 and A in CePtAl.

are three successive magnetic transitions at T_1=5.9 K, T_2=4.3 K and T_3=2.2 K [1,2]. The present experiments were performed using a cubic -anvil cell at pressures up to 8.0 GPa in the temperature range from 2 to 300 K.

Figure 1 shows the temperature dependence of electrical resistivity at several pressures. At ambient pressure, the resistivity has a broad hump centered at approximately 150 K and decreases steeply below the ordering temperature T_1=5.9 K. The broad hump is due to a combined effect of the Kondo effect and the crystalline electric field effect. With increasing pressure, T_1 increases slightly and the broad hump is shifted to lower temperature and another broad hump appears below 20 K. This hump seems to be enhanced with increasing pressure. The former broad hump and the latter hump are merged into a shoulder-like hump at pressures higher than 6.0 GPa. The temperature at which the merged hump is centered increases with increasing pressure. This behavior above 6.0 GPa is often observed in a heavy fermion compound such as $CeAl_3$, indicating a valence fluctuating state. The ordering temperature T_1 increases slightly with increasing pressure. Interestingly, the ordering state disappears abruptly above 6 GPa, indicating a first-order like phase transition of an electronic state from a heavy fermion state to the valence fluctuating state. Figure 2 shows the pressure dependences of T_1, the residual resistivity ρ_0 and the coefficient A of the T^2-dependence in electrical resistivity. Both ρ_0 and A increase as functions of pressure up to 5 GPa.

A=2.4μΩcm/K^2 at 5 GPa is larger than the value of the heavy fermion superconductor UPt_3. A characteristic feature in CePtAl is that marked changes in ρ_0 and A are found in a very narrow pressure region from 5.0 to 6.0 GPa. Correspondingly, the ordering temperature does not decrease smoothly as a function of pressure, but becomes zero abruptly. These results suggest that a first-order phase transition is realized in CePtAl.

References

[1] A. Dönni, H. Kitazawa, P. Fischer, J. Tang, M. Kohgi, Y. Endo, and Y. Morii, J. Phys.: Condens. Matter **7**, 1663 (1995).
[2] H. Kitazawa, S. Nimori, J. Tang, F. Iga, A. Dönni, T. Matsumoto, and G. Kido, Physica B **237-238**, 212 (1997).
[3] H. Kitazawa, A. Dönni, L. Keller, J. Tang, F. Fauth, and G. Kido, J. Solid State Chem. **140**, 233 (1998).
[4] K. Miyake and H. Maehashi, J. Phys. Soc. Jpn. **71**, 1007 (2002).

Authors

T. Ueda, M. Nakashima, M. Hedo, Y. Uwatoko, H. Nakashima, A. Thamizhavel, T. D. Matsuda, Y. Haga, R. Settai, and Y. Onuki.

Ultra-Large-Scale Electronic Structure Theory and Nano-Structure Process

T. Hoshi and T. Fujiwara

We have developed a set of theories and program codes in ultra-large-scale electronic structure calculations, particularly, for process of nano structures, structures in nano-meter or ten-nano-meter scales [1-5]. In the test calculations of Fig.1, the computational cost of our methods shows the 'order-N' or linear-scaling property with the system size (N), up to ten-million atoms. The common theoretical foundation of our methods is the quantum-mechanical calculation of the one-body density matrix or the Green's function, instead of one-electron eigenstates. Practical calculations were carried out using Hamiltonians in the Slater-Koster form.

As an application, 10-nm-scale molecular dynamics simulation was carried out for surface formation process in silicon cleavage [1, 3, 5]. As shown in Fig.2, we obtained not only the elementary formation process of the (experimentally observed) (111)-(2×1) surface but also step formation and bending of cleavage path. These results are consistent to experiments and capture the dynamical aspect of cleavage, which is beyond the traditional understanding with surface

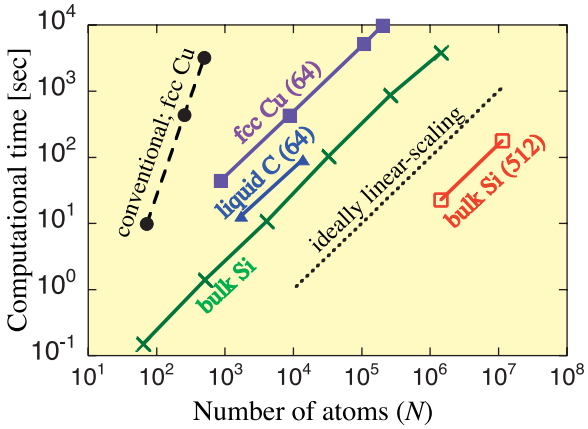

Fig. 1. The ultra-large-scale calculation with up to 11,315,021 atoms; [1,3,5] The computational time of our methods is plotted for fcc Cu and liquid C with 64 CPUs and for bulk Si with single CPU and 512 CPUs. The time of the conventional eigenstate calculation is also plotted for fcc Cu with single CPU. The computations were carried out using Intel or SGI CPUs.

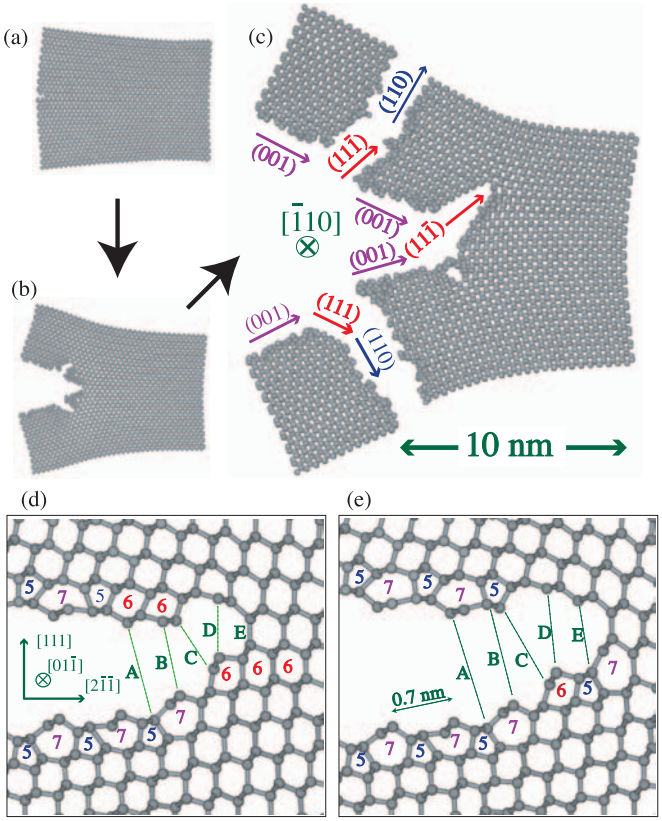

Fig. 2. Surface formation process in silicon cleavage; [3] (a)-(c): Bending of cleavage path into the experimentally observed ((111) or (110)) planes. The present snapshots describe a process on the order of 10 ps. (d)-(e): Two successive snapshots with the time interval of 0.6 ps. A pair of five- and seven-member rings is the unit structure of the experimentally observed (111)-(2 × 1) surface, called Pandey structure. A step structure appears with a six-member ring. Bond sites in the initial (crystalline) structure are indicated by letters, such as 'A' and 'B'.

energy [3]. Moreover, the local density of states, calculated from the Green's function [4], shows characteristic surface states at the step-edge region, which reproduce bias-dependent STM image [5]. The step structures are experimentally observed but their explicit atomic structures have not been settled. In conclusion, our results propose a promising candidate of the step structure and should be confirmed experimentally.

In general, the variety of structure and function in nano systems stems from the competition of bulk and non-bulk parts whose electronic states are essentially different. The present electronic-structure theory reproduces this competition, as in the above application [3], and enables us systematic investigations of nano-structure processes among different materials and phenomena. Other applications are now proceeding.

References

[1] T. Hoshi and T. Fujiwara, J. Phys. Soc. Jpn. **72**, 2429 (2003).
[2] R. Takayama, T. Hoshi, and T. Fujiwara, J. Phys. Soc. Jpn. **73**, 1519 (2004).
[3] T. Hoshi, Y. Iguchi, and T. Fujiwara, Phys. Rev. B **72**, 075323 (2005).
[4] R. Takayama, T. Hoshi, T. Sogabe, S.-L. Zhang, and T. Fujiwara, Phys. Rev. B **73**, 165108 (2006).
[5] T. Hoshi, R. Takayama, Y. Iguchi, and T. Fujiwara, Physica B **376-377**, 975 (2006).

Authors

T. Hoshi[a] and T. Fujiwara[a],
[a]University of Tokyo.

Oxygen Non-Stoichiometry in the Mixed Valence RBaCo$_4$O$_{7+\delta}$ (R: Dy-Lu, Y) Systems

N. Nakayama and Y. Ueda

Mixed valence cobalt oxides, RBaCo$_4$O$_{7+\delta}$ (R: Dy-Lu, Y; hexagonal $P6_3mc$ or trigonal $P31c$), show interesting successive structural and magnetic phase transitions [1, 2]. Barium and oxygen atoms compose a 4H($abac$)-type closed packed BaO_7 sublattice. Cobalt and R atoms occupy the tetrahedral and the octahedral sites, respectively. CoO_4 tetrahedra link their corners to form a 3-dimensional network, in which 2-dimensional Co *kagomé* and triangular lattices are stacked alternately. The magnetic frustration and the charge ordering may feature in the structural and magnetic phase transitions, although the details have not been clarified yet.

Another interesting property is the oxygen non-stoichiometery with the highly excess amount. For example, LuBaCo$_4$O$_7$, when annealed in 1 atm of oxygen stream at 300 ºC, topochemically absorbs oxygen up to the composition of LuBaCo$_4$O$_{7.8}$. The reversible oxygen absorption and desorption occur at around 350 ºC. The crystal lattice shows an anisotropic shrinkage on oxygen absorption; the a-axis shows 0.4% contraction and the c-axis is almost unchanged. The sample with the excess oxygen does not show any structural phase transitions and the magnetic susceptibility suggests somewhat glassy magnetic ordering.

The excess oxygen atoms chemically order at room temperature. Figure 1 shows an electron diffraction pattern and a HREM lattice image of LuBaCo$_4$O$_{7.8}$. The structural modulation is clearly seen along the <110> direction of the fundamental $P6_3mc$ lattice with a period of 1.88 nm: six times of the (110) lattice spacing. The Yb and Tm compounds also show the similar oxygen over-stoichiometry and the chemical ordering. The Er, Ho, Dy, and Y compounds with the larger R atoms form the more over-stoichiometric phases with the composition around RBaCo$_4$O$_{8.3}$. However, on oxygen absorption, the crystal lattice shrinks along the c-axis and expands in the a-plane as shown in Fig. 2. The period of the chemical ordering also turns to the ten times of the (110) lattice spacing. Because Ba and O atoms are well assumed to form the closed packed BaO_7 lattice, there is no room to accept the excess oxygen composition. This means that the excess O atoms occupy the interstitial sites in the closed packed lattice. However, the

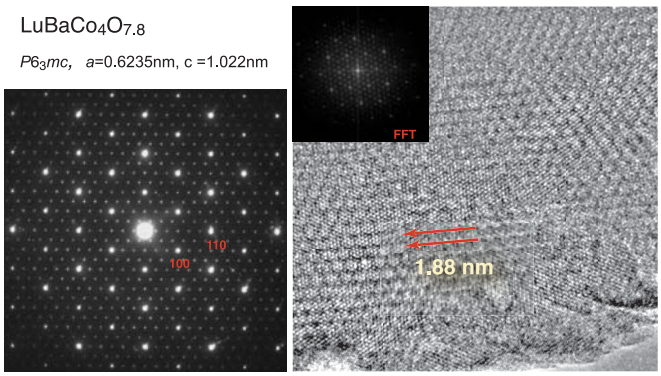

Fig. 1. An electron diffraction pattern and a lattice image of over-stoichiometric LuBaCo$_4$O$_{7.8}$. The excess oxygen atoms form a chemical superlattice at room temperature with a period of 1.88 nm along the <110> direction of hexagonal fundamental lattice with $P6_3mc$ symmetry (a = 0.6235nm, c = 1.0220nm). The electron beam incidence is parallel to the c-axis.

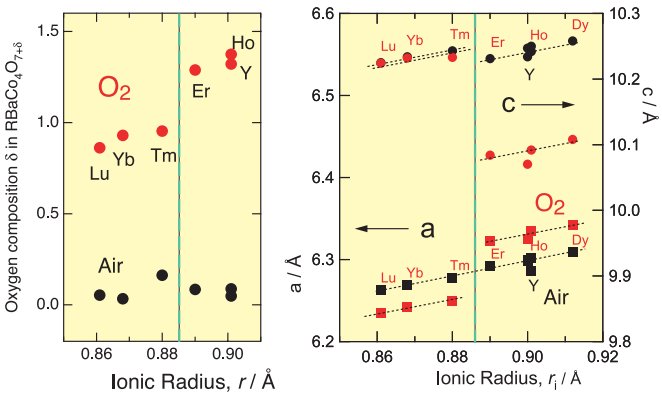

Fig. 2. Oxygen compositions and lattice parameters of over-stoichiometric RBaCo$_4$O$_{7+\delta}$ (R: Dy-Lu, Y). Lattice parameters of nearly stoichiometric RBaCo$_4$O$_7$ are also shown (black marks). Note the anisotropic lattice shrinkage on oxygen absorption and also the dependence on the ionic size of R.

details of the ordered structure are unknown. The neutron diffraction study is in progress.

References
[1] M. Valldor, Solid State Sci. **6**, 251 (2004).
[2] N. Nakayama, T. Mizota, Y. Ueda, A. N. Sokolov, and A. N. Vasiliev, J. Magn. Magn. Mater. **300**, 98 (2006)

Authors
N. Nakayama[a], T. Nakajima, and Y. Ueda
[a]Yamaguchi University

Preparation and Magnetic Properties on A$_{0.33}$Sr$_{0.67}$CoO$_{3-\delta}$ (A = Y, Gd)

Y. F. Zhang, M. Izumi, and Y. Kiuchi

Recently, extensive studies have been carried out on the cobalt oxide due to its unique magnetic behaviors and various spin state [1-2], LS (low spin) state, IS (intermediate spin) state and HS (high spin) state. By the theoretical calculation in the perovskite LaCoO$_3$ [2], the e_g orbital ordering exists in the IS state configuration. The cobaltite RBaCo$_2$O$_{5-d}$ can have Co-O octahedron, square pyramid or both structures depending on the amount of oxygen [1, 2]. The unusual paramagnetic (PM) reentrant phenomenon on the GdBaCo$_2$O$_{5-d}$ compound that occurs via a couple of spin-state transition has been reported [1]. In our work, we choose the nonmagnetic Y ion and magnetic Gd ion to prepare A$_{0.33}$Sr$_{0.67}$CoO$_{3-d}$ (A = Y, Gd) samples by the conventional solid state reaction technique to study structural and magnetic properties.

The homogeneity and stoichiometry of the samples were analyzed by the electron-probe microanalysis (EPMA) and inductively coupled plasma (ICP) spectroscopy which confirmed that the compositions were Y : Sr : Co = 0.323 : 0.672 : 1 and Gd : Sr : Co = 0.345 : 0.699 : 1. The oxygen content

Table 1. The lattice parameters, the average Co-O bond length, deduced from the Rietveld refinement of XRD data at room temperature for A$_{0.33}$Sr$_{0.67}$CoO$_{3-d}$ (A=Y, Gd) samples (space group=I4/mmm). Here iodometric titration data shown include the standard deviation.

Sample	a (A)	c (A)	Co1-O	Co2-O	A:Sr: Co ratio	3-d	Co valence
Y$_{0.33}$Sr$_{0.67}$CoO$_{3-d}$	7.6164	15.2747	1.9064	1.9810	0.323: 0.672 :1	2.614(3)	2.917
Gd$_{0.33}$Sr$_{0.67}$CoO$_{3-d}$	7.6272	15.3082	1.8676	1.9972	0.345: 0.699:1	2.824(0)	3.215

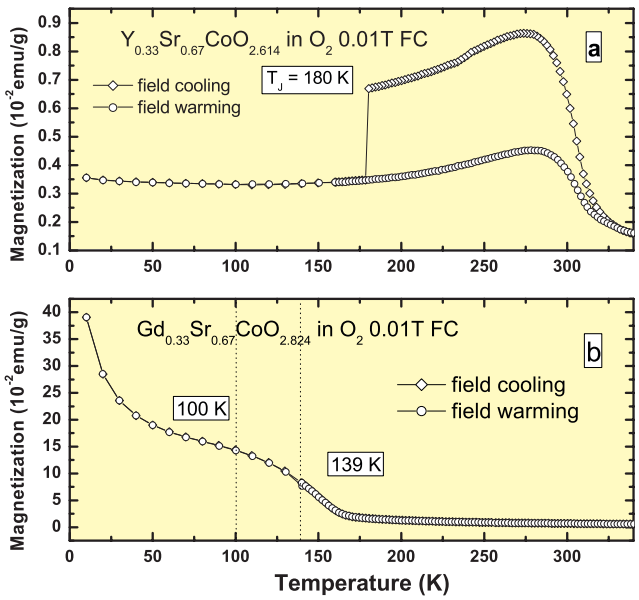

Fig. 1. (a) Field magnetization vs temperature curve of $Y_{0.33}Sr_{0.67}CoO_{2.614}$ at 0.01 T. (b) Field magnetization vs temperature curve of $Gd_{0.33}Sr_{0.67}CoO_{2.824}$ at 0.01 T.

was determined through iodometric titration [3]. The Rietveld profile analysis of the XRD pattern reveals the two compounds have a common perovskite-based structure (Table 1). Two Co ions form layered alternating order of CoO_4 tetrahedron and CoO_6 octahedron [4]. The average charge valence in $Y_{0.33}Sr_{0.67}CoO_{2.614}$ is 2.917, implying that 8% of cobalt ions are in Co^{2+} and the rest of them are in Co^{3+}. However, in $Gd_{0.33}Sr_{0.67}CoO_{2.824}$ the averaged charge of Co ions is 3.215, implying that about 8% of cobalt ions are in Co^{4+} and the rest of them are in Co^{3+}. The different oxygen contents between two compounds would lead to different magnetic properties.

Figure 1 (a) shows the magnetization versus temperature data of $Y_{0.33}Sr_{0.67}CoO_{2.614}$ sample under an applied field of 0.01 T. There is a DC magnetization jump (T_J) at about 180 K during the magnetic field cooling, and subsequently the magnetization normally returns to the high temperature, indicating a kind of magnetic memory effect. The magnetization decrease is correlated to the AFM appearance in IS spin state. The phase transition from FM to AFM at T_J is not simply interpreted as the spin-state transition; we should consider the orbital ordering of e_g electron suggested by Korotin et. al [2]. The IS state configuration is e_g^1. Due to the strong Jahn-Teller nature of this configuration, this state may be a source of the ordering of orbital. It supports the fact that the spin structure in AFM state may take a FM ordering in-plane but AFM ordering interplane. With temperature increase, there is higher Curie temperature at about 304 K.

The complicated magnetic behavior of Gd-doped sample is shown at Fig. 1(b), where magnetization jump does not appear. It is PM behavior above 139 K, shows a FM transition near 139 K (T_C), and develops like a ferromagnet down to about 100 K. Below 100 K, the magnetization increases like a typical PM phase, which is similar to the phenomena in $GdBaCo_2O_{5+d}$ [1]. We suggested that reentrant PM transition at about 100 K is mainly due to the spin state transition from IS to LS state of Co^{3+} ions.

A comparative study of both Y-doped and Gd-doped cobaltites with different populations of cobalt ions as well as spin states may give a new kind of phase transition under regulated oxygen contents.

References

[1] W. S. Kim, E. O. Chi, H. S. Choi, N. H. Hur, S. -J. Oh, and H. -C. Ri, Solid State Commun. **116**, 609 (2000).
[2] M. A. Korotin, S. Yu. Ezhov, I. V. Solovyev, and V. I. Anisimov, Phys. Rev. B **54**, 5309 (1996).
[3] M. Karppinen, M. Matvejeff, K. Salomäki, and H. Yamauchi, J. Mater. Chem. **12**, 1761 (2002).
[4] S. Ya. Istomin, J. Grins, G.Svensson, O. A. Drozhzhin, and E. V. Antipov, Chem. Mat. **15**, 4012 (2003).

Authors

Y. F. Zhang[a], S. Sasaki[a], O. Yanagisawa[b], M. Izumi[a], and Y. Kiuchi
[a]Tokyo University of Marine Science and Technology
[b]Yuge National College of Maritime Technology

ISSP Workshop

1. Rattling and superconductivity

May 9, 2005

Z. Hiroi

The Workshop was held on May 9, 2005 to discuss on the rattling phenomena and its relation to the occurrence of superconductivity in several classes of compounds like filled-skutterudite, clathrate and pyrochlore compounds. About 50 people attended, and 14 lectures were presented. The rattling phenomena have recently attracted many interests because it is believed to suppress the thermal conductivity and thus give rise to a large thermoelectric figure of merit in application study. However, the physical meaning of this effect is still under debate and to be clarified in various materials. Particularly, the influence of the rattling motion to conducting carries in the surrounding cage is an interesting topic, which was discussed extensively in this Workshop.

http://www.issp.u-tokyo.ac.jp/contents/seminar/short/tanki20050509.html

2. Evolution of high magnetic field research on condensed matter utilizing micro-probes

June 13-14, 2005

M. Hagiwara

In this meeting, we discussed recent results of research on condensed matter physics in high magnetic fields, such as strongly correlated electron systems, quantum spin systems, semiconductors, molecular conductors and so on. In particular, we discussed a future plan and evolution of neutron and x-ray scattering experiments in high magnetic fields as central topics of this meeting.

http://www.issp.u-tokyo.ac.jp/labs/extreme/himag-forum/page006.html

3. Neutron scattering under high pressures

July 22, 2005

K. Hirota, M. Nishi, Y. Uwatoko, H. Amitsuka, and H. Yoshizawa

It is more than 15 years since the JRR-3 research reactor, a center of neutron science in Japan, was built in Tokai. Many efforts have been being given to renovate and sophisticate the instruments recently. As to triple-axis spectrometers, the ISSP Neutron Science Laboratory has refurbished them with a completely new control system, and introduced two sets of new liquid-He-free 1K cryostat to expand the temperature range easily accessible for our users. For a couple of years, we also have been developing new high pressure cells which have higher neutron transmittance and are easy to use. Since this year, we have started constructing neutron focusing devicec using supermirrors to obtain a focused and intense neuron beam required for high pressure experiments on triple-axis spectrometers. Motivated by these rapid technological advancements, we had a one-day workshop to discuss “neutron scattering under high pressures”, particularly focusing upon possibilities for studying d and f electron systems as well as relaxor ferroelectrics, and new types of high pressure equipments applicable to these issues.

To our welcome surprise. more than 50 participants have attended to this meeting despite the condition that the workshop was held in Tokai and that only a month was given for preparation. 16 lectures were given by invited speakers: In the beginning, sophistication of neutron spectrometers, development of neutron focusing devices and new high pressure cells for neutron scattering were discussed. Then, various recent experimental research works were presented, many of which utilize neutrons from reactors combined with complementary techniques such as synchrotron radiations, ?SR and pulse neutrons. These talks were followed by experimental challenges for higher pressures with lower temperatures. In the end, a series of lectures were given for several materials, which are expected to show novel anomalies under high pressures. We were all overwhelmed by enthusiastic talks and following discussions. We have realized that high pressure experiments are frontiers for not only neutron scattering but also all kinds of beam line sciences: This consensus will be a driving force for constructing a new scientific field through collaborations among the participants.

http://www.issp.u-tokyo.ac.jp/contents/seminar/short/tanki20050722.html

4. Hydrogen in solids

Nov. 24-25, 2005

K. Fukutani, K. Aoki, S. Ikeda, M. Kubota, H. Sugimoto, S. Tsuneyuki, and J. Yoshinobu

Hydrogen in solids dramatically affects the electronic, structural and mechanical properties of solids as realized in hydrogen embrittlement, H-storage, and H-induced metal-insulator transition. Due to the light mass and nuclear spin, hydrogen frequently reveals particular quantum effects such as tunneling, zero-point vibration, extended features of the nuclear wavefunction.

The research area related hydrogen interacting with solids encompasses metals, semiconductors, dielectrics, surfaces and interfaces, solid hydrogen, high-pressure physics, low-temperature physics and so on. Reflecting the increasingly sophisticated range of experimental and theoretical techniques, much progress has been made in the understanding of hydrogen transport, reactivity, and correlations with electronic and structural properties. Exotic beams including positron, muon, and anti-hydrogen, are broadening the field as an interdisciplinary research area.

This workshop highlighted the topics of each area in aimed at promoting mutual communications between different communities. A total of 180 scientific delegates attended the workshop from all over Japan and 20 invited talks pointing to current status and directions of the research area were presented. One-minute presentations by the poster presenters stimulated extended and excited discussions.

http://bilbo.phys.s.u-tokyo.ac.jp/hydrogen/

5. Theory of electronic structure calculations and application for new nano-scale electronics

December 26-27, 2005

K. Kusakabe

Intending to find new functionality in characteristics of materials at around the phase transition, much attention is paid for the correlated electron systems. For this purpose, development in the first-principles electronic structure calculations is required. This is because, for the design of materials based on the precise quantum mechanical analysis, only the ab-initio method is able to give the materials solution. Proper treatment of non-local correlation effects due to both short-ranged and long-ranged correlations in electronic systems, large scale simulation in both length and time scales, and other recognized problems are now gradually solved. Response to the outer electro-magnetic fields is rather nicely described in the first-principles calculations, so that the full-quantum-mechanical device simulation is now available. This ISSP workshop was thus planned to discuss recent rapid progress of the electronic structure calculation and to review achievement in theoretical techniques. The program contained 34 aural presentations and 16 posters and over 100 participants were attended and over 100 participants were took part in active discussion. In addition, a special panel discussion was held. The panel discussion was entitled ‘prospects and expectations of the peta-flops machines in the condensed matter physics’.

http://www.issp.u-tokyo.ac.jp/public/ISSP_WS_20051226/